Acceleration feedback control of human-induced floor vibrations

Iván M. Díaz [a, *], Paul Reynolds [b]

[a] *Escuela Técnica Superior de Ingenieros Industriales, Universidad de Castilla-La Mancha, Edificio Politécnico, Av. Camilo José Cela s/n, 13071, Ciudad Real, Spain*

[b] *Department of Civil and Structural Engineering, The University of Sheffield, Sir Frederick Mappin Building, Mappin Street, Sheffield, S1 3JD, United Kingdom*

[*] Corresponding author: Tl.: +34926295238; Fax: +34926295300; E-mail: Ivan.Munoz@uclm.es

Abstract

Active vibration control (AVC) via a proof-mass actuator is considered to be a suitable technique for the mitigation of vibrations caused by human motions in floor structures. It has been observed that actuator dynamics strongly influence structure dynamics despite considering collocated actuator/sensor control. The well-known property of the interlacing of poles and zeros of a collocated control system is no longer accomplished. Therefore, velocity-based feedback control, which has been previously used by other researchers, might not be a good solution. This work presents a design process for a control scheme based on acceleration feedback control with a phase-lag compensator, which will generally be different from an integrator circuit. This first-order compensator is applied to the output (acceleration) in such a way that the relative stability and potential damping to be introduced are significantly increased accounting for the interaction between floor and actuator dynamics. Additionally, a high-pass filter designed to avoid stroke saturation is applied to the control signal. The AVC system designed according to this procedure has been assessed in simulation and successfully implemented in an in-service open-plan office floor. The actual vibration reductions achieved have been approximately 60% for walking tests and over 90% for a whole-day vibration monitoring.

Key words: Active control; Structural control; Floor vibration; Saturated control; Acceleration feedback; Human-induced vibration

1. Introduction

Advances in structural technologies have enabled the design of light and slender structures, which have increased susceptibility to vibration. This is compounded by the trend toward open-plan floor structures, which have less inherent damping. Examples of notable vibrations under human-induced excitations have been reported in office buildings, footbridges, shopping malls and sport stadia, amongst other structures. Such vibrations can cause a serviceability problem in terms of disturbing the users, but they rarely affect the fatigue behaviour or safety of structures [1].

Passive and semi-active devices have been proposed to reduce floor vibrations [2] [3]. However, due to their passive nature, the vibration cancellation is often of limited effectiveness and they often have to be tuned to damp a single vibration mode. In many cases, several of these devices have to be used to achieve the required vibration reduction. Instead, an active control approach rather than passive devices might be more effective [4]. A state-of-the-art review of technologies (passive, semi-active and active) for mitigation of human-induced vibration can be found in [5]. Furthermore, techniques to cancel floor vibrations (especially passive and semi-active techniques) are reviewed by Ebrahimpour and Sack [6].

An AVC system based on direct velocity feedback control (DVFC) with saturation has been studied analytically and implemented experimentally for the control of floor vibrations induced by humans via a proof-mass actuator [7] [8]. This actuator generates inertial forces in the structure without need for a fixed reference. The velocity output, which is obtained by an integrator circuit applied to the measured acceleration response, is multiplied by a constant gain and feeds back to a collocated force actuator. The merits of this method are its robustness to spillover effects due to high-order unmodelled dynamics and that it is unconditionally stable in the absence of actuator and sensor (integrator circuit) dynamics [9]. That is, the resulting root locus map exhibits the well-known interlacing property of poles and zeros of collocated systems [10]. However, when these dynamics are considered, the interlacing property is no longer accomplished. Then, DVFC is not such a desirable solution. Furthermore, the control law is completed by a command limiter (i.e., a saturation nonlinearity in the command signal) that is introduced to avoid actuator force and stroke saturation and to level off the system response in the case of unstable behaviour.

It has been shown that the use of a proof-mass actuator, even though this is positioned at the same location as the sensor, leads to a non-collocated root locus map. The actuator dynamics introduce a pair of

high-damped poles that affect drastically the loci corresponding to the structure dynamics [7] [10] [11]. This fact might reduce importantly the stability margins and the possible damping to be introduced by the AVC system. Moreover, the closed-loop system could be very sensitive to parameter uncertainties since the control gain should be carefully chosen. For example, in [7], it was shown that a couple of branches in the root locus corresponding to the actuator dynamics go to the right-half plane provoking unstable behaviour in the actuator. The saturation avoids this unstable behaviour but the actuator is involved in a stable limit cycle [12], which is not desirable since it could result in dramatic effects on the system performance and its components. Generally, depending on the interaction between floor and actuator dynamics, one of them will tend to be unstable. Thus, the selection of a suitable compensator to be applied to the actual measured output that ensures high stability margins and enables potentially the introduction of significant damping via closed-loop control is an interesting issue to be dealt with.

This paper presents a design process of a compensator to be applied to the acceleration output of a structure. It is assumed that the output of the structure is the acceleration, which is usually the actual magnitude measured. This compensator accounts for the interaction between the structure and the actuator dynamics in such a way that it introduces the phase-lag needed to achieve a closed-loop system with desirable properties. Such properties are high damping for the fundamental vibration mode of the structure and high stability margins. Both properties lead to a closed-loop system robust with respect to stability and performance [10]. Acceleration feedback with the phase-lag compensator will be referred as to compensated acceleration feedback control (CAFC) throughout the paper. The proposed design process is completed by: 1) a phase-lead (high-pass property element) compensator which prevents the actuator stroke saturation at low frequencies, and 2) a saturation nonlinearity applied to the control signal to avoid actuator force overloading at any frequency. This phase-lead compensator (direct compensator from this point onwards) must be designed before the design of the phase-lag compensator (feedback compensator from this point onwards) in order to account for the dynamics introduced by the former in the design of the latter. Additionally, the design process is simple since the direct compensator is derived from a frequency domain analysis and the feedback compensator is obtained using the root locus method.

The remainder of this paper is organized as follows. The general control strategy together with floor and actuator dynamics are briefly described in Section 2. The control design procedure is presented in Section 3. Section 4 deals with the experimental implementation of the AVC system in an in-service open- plan office floor. This section contains the system dynamic models, the application of the proposed

design procedure, simulation results to assess the feasibility of the design and experimental results involving walking tests and whole-day monitoring tests to quantify the actual vibration reductions. Finally, some conclusions and suggestions for future work are given in Section 5.

2. Control strategy and system dynamics

The main components of the general control strategy adopted in this work are shown in Fig. 1. The output of the system is the structural acceleration since this is usually the most convenient quantity to measure. Because it is rarely possible to measure the system state and due to simplicity reasons, direct output measurement feedback control might be preferable rather than state-space feedback in practical problems [13]. In this figure, G_A is the transfer function of the actuator, G is of the floor structure, C_D is of the direct compensator and C_F is of the feedback compensator. The direct one is merely a phase-lead compensator (high-pass property) designed to avoid actuator stroke saturation for low-frequency components. It is notable that its influence in the global stability will be small since only a local phase-lead is introduced. The feedback one is a phase-lag compensator designed to increase the closed-loop system stability and to make the system more amenable to the introduction of significant damping by a closed-loop control. The control law is completed by a nonlinear element $f(\ddot{y}_c)$ that may be a saturation nonlinearity to account for actuator force overloading [4], an on-off nonlinearity with a dead zone [12] or a variable gain with a switching-off function [14]. In this work, a saturation nonlinearity will be assumed.

2.1. Floor dynamics

If one considers the collocated case between the acceleration (output) and the force (input) and using the modal analysis approach, the transfer function of the floor dynamics can be represented as an infinitive sum of second-order systems as follows [10]

$$G(s)=\sum_{i=1}^{\infty}\frac{\chi_i s^2}{s^2+2\xi_i\omega_i s+\omega_i^2}, \tag{1}$$

where $s=j\omega$, ω is the frequency, χ_i, ξ_i and ω_i are the inverse of the modal mass, damping ratio and natural frequency associated to the ith mode, respectively. For practical application, N vibration modes are considered in the frequency bandwidth of interest. The transfer function $G(s)$ is thus approximated by a truncated one

$$\tilde{G}(s)=\sum_{i=1}^{N}\frac{\chi_i s^2}{s^2+2\xi_i\omega_i s+\omega_i^2}\,. \tag{2}$$

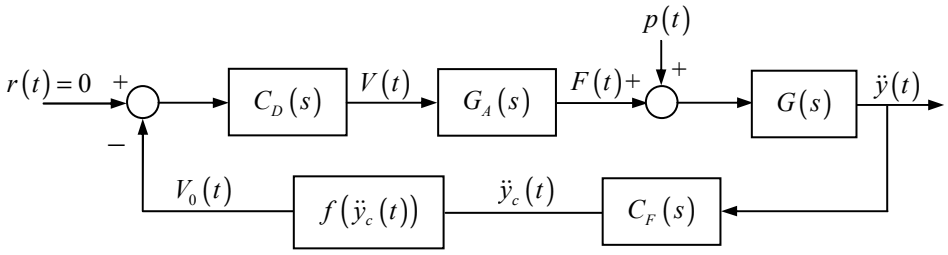

$r(t)$	Reference command	$\ddot{y}(t)$:	Acceleration response
$V(t)$:	Control voltage	$\ddot{y}_c(t)$:	Compensated acceleration
$F(t)$:	Actuator force	$V_0(t)$:	Initial control voltage
$p(t)$:	Plant disturbance	$f(\ddot{y}_c)$:	Nonlinear element

$C_D(s)$: Transfer function of the direct compensator

$G_A(s)$: Transfer function of the proof-mass actuator

$G(s)$: Transfer function of the floor structure

$C_F(s)$: Transfer function of the feedback compensator

Fig. 1. General control scheme.

2.2. Proof-mass actuator dynamics

The linear behaviour of a proof-mass actuator can be closely described as a linear third-order model. Unlike previous works [4], [12], a low-pass element is added to a linear second-order system in order to account for the low-pass property exhibited by these actuators. The cut-off frequency of this element is not always out of the frequency bandwidth of interest since it is approximately 10 Hz [15]. Such a low-pass behaviour might affect importantly the global stability of the AVC system. Thus, the actuator is proposed to be modelled by

$$G_A(s)=\left(\frac{K_A s^2}{s^2+2\xi_A\omega_A s+\omega_A^2}\right)\left(\frac{1}{s+\varepsilon}\right)=\frac{K_A s^2}{s^3+(2\xi_A\omega_A+\varepsilon)s^2+(2\xi_A\omega_A\varepsilon+\omega_A^2)s+\varepsilon\omega_A^2}\,, \tag{3}$$

where $K_A>0$, and ξ_A and ω_A are, respectively, the damping ratio and natural frequency which take into consideration the suspension system and internal damping. The pole at $-\varepsilon$ provides the low-pass property.

3. Controller design

The purpose of this section is to provide a procedure to design the compensators C_D and C_F (see Fig. 1). The design of C_D is undertaken in the frequency domain and the design of C_F is carried out through the root locus technique. The root locus maps the complex linear system roots of the closed-loop transfer function for control gains from zero (open-loop) to infinity [16]. In the design of C_F, it is assumed that the natural frequency of the actuator ω_A (see Eq. (3)) is sufficiently below the first natural frequency of the structure ω_1 (see Eq. (2)) in such a way that no pole-zero flipping can take place. Typically, it can be considered that ω_A is less than half of ω_1 [17].

3.1. Direct compensator

The transfer function between the moving mass displacement and input voltage to the actuator can be considered as follows

$$G_d(s) = \frac{1}{m_A}\frac{G_A(s)}{s^2}, \tag{4}$$

with m_A being the mass of the moving mass. Fig. 2a shows an example of magnitude of G_d. The moving mass displacement at low frequencies should be limited due to stroke saturation. A transfer function with the following magnitude is defined

$$\left|\hat{G}_d(j\omega)\right| = \begin{cases} d & 0 \le \omega \le \hat{\omega} \\ \left|G_d(j\omega)\right| & \hat{\omega} < \omega < \infty \end{cases}, \tag{5}$$

in which *d* is the maximum allowable stroke per unit voltage and $\hat{\omega}$ is the higher frequency that fulfils $\left|G_d(j\hat{\omega})\right| = d$. A high-pass compensator of the form

$$C_D(s,\lambda,\eta) = \frac{s+\lambda}{s+\eta} \text{ with } \eta > \lambda \ge 0, \tag{6}$$

is applied to the initial control voltage $V_0(t)$ and its output is the filtered input to the actuator $V(t)$ (see Fig. 1). Fig. 2b shows an example of C_D. The following error function is defined

$$e(\omega,\lambda,\eta) = \left(\left|\hat{G}_d(j\omega)\right| - \left|C_D(j\omega,\lambda,\eta)\,G_d(j\omega)\right|\right)^2, \tag{7}$$

with $\omega \in (\omega_L, \omega_U)$, $\omega_L < \hat{\omega}$, $\omega_U > \hat{\omega}$, and ω_L and ω_U being, respectively, the lower and upper value of the frequency range to be considered in the design. The lower frequency ω_L must be selected in such a way that the actuator resonance is sufficiently included and the upper frequency ω_U must be chosen so that the floor dynamics that are prone to be excited are included. Parameters λ and η of the compensator are obtained by minimising the error function (7)

$$\min_{(\lambda,\eta) \in \mathbb{R}^+} e(\omega, \lambda, \eta), \forall \omega \in (\omega_L, \omega_U), \tag{8}$$

with $\lambda \in [0, \lambda_{\max})$, $\eta \in (0, \eta_{\max})$, $\eta_{\max}, \lambda_{\max} \leq \varepsilon$, and $\lambda_{\max}$ and $\eta_{\max}$ being, respectively, the maximum considered value of λ and η for the optimisation problem (8). Note that λ and η are delimited by the low-pass property of the actuator ε in order to minimise the influence of C_D on the global stability properties. By and large, the objective is to fit $C_D(j\omega)G_d(j\omega)$ to *d* for $\omega_L \leq \omega \leq \hat{\omega}$ and not to affect the dynamics for $\hat{\omega} < \omega < \omega_U$ (see Fig. 2a). The result is a high-pass compensator that introduces dynamics mainly in the frequency range $\omega_L \leq \omega \leq \hat{\omega}$ in such a way that the global stability is not compromised. Note that sharper high-pass filter could be used but the penalty due to introduced phases might not be negligible and the global stability might be compromised.

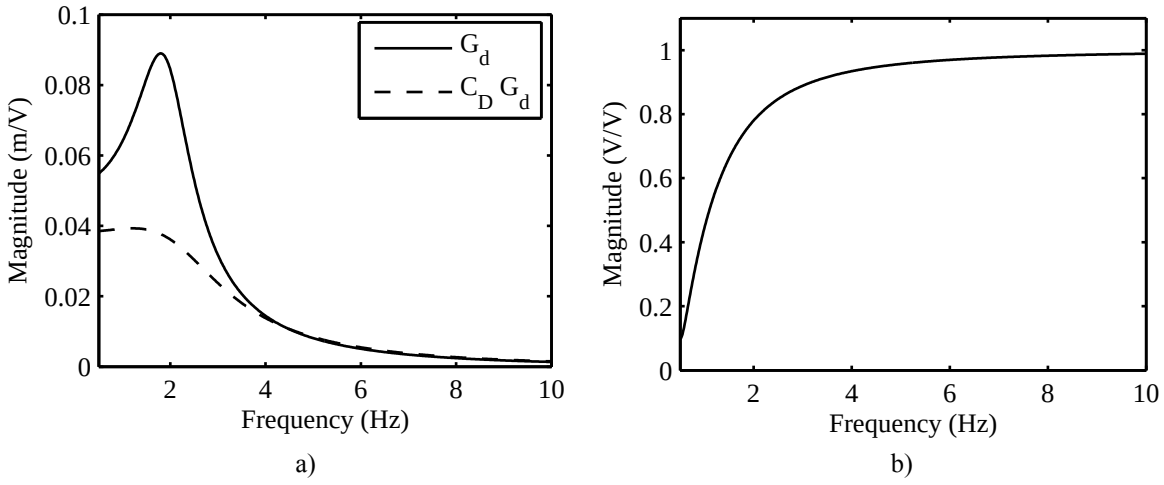

Fig. 2. Effect of the high-pass compensator on the actuator dynamics. a) Magnitude of G_d and $C_D G_d$. b) Magnitude of C_D.

3.2. Feedback compensator

To illustrate the selection of the form of the compensator C_F, the root locus map (*s*-plane) for four different cases is shown in Fig. 3. A realistic structure is assumed with two significant vibration modes. The modal mass and damping ratio for both modes are assumed to be 20 tonnes and 0.03, respectively. The four cases are: a) direct acceleration feedback control (DAFC) considering two vibration modes at 4 and 10 Hz, respectively; b) DVFC for the same structure as in a); c) DAFC considering two vibration modes at 7 and 10 Hz, respectively; and d) DVFC for the same structure as in c). The actuator dynamics (Eq. (3)) is represented by a pair of high-damped poles, two zeros at the origin and a real pole and the structure is represented by two zeros at the origin and interlacing low-damped poles and zeros. It is clearly shown that the resulting root locus has non-collocated system features due to the influence of the actuator dynamics on the structure dynamics. On one hand, it is observed that for a floor with a low fundamental frequency (4 Hz), direct output feedback (DAFC since the actual measurement is the acceleration) will provide very small relative stability (the distance of the poles to the imaginary axis in the *s*-plane [16]) and low damping. However, the inclusion of an integrator circuit (a pole at the origin for an ideal integrator), which results in DVFC, improves substantially such properties. On the other hand, for a floor with a higher fundamental frequency (7 Hz), DAFC provides much better features than DVFC.

Fig. 3 shows the fact that DVFC might not be a good solution and supports the use of CAFC. It is therefore proposed to apply the following phase-lag compensator to the measured acceleration

$$C_F(s) = \frac{s+\gamma}{s} \text{ with } \gamma \geq 0. \tag{9}$$

If $\gamma = 0$, the control scheme will be DAFC. If $\gamma \gg \varepsilon$, which means that the zero of the compensator does not affect the dominant system dynamics, the control scheme will then be considered DVFC. Parameter γ has to be chosen according to the closed-loop poles corresponding to the fundamental frequency of the floor in order to: 1) improve substantially their relative stability, 2) decrease their angles with respect to the negative real axis to allow increasing damping, and 3) increase the distance to the origin to allow increasing natural frequency. Note that increasing values both of the frequency and the damping result in decreasing the settling time of the corresponding dynamics [16].

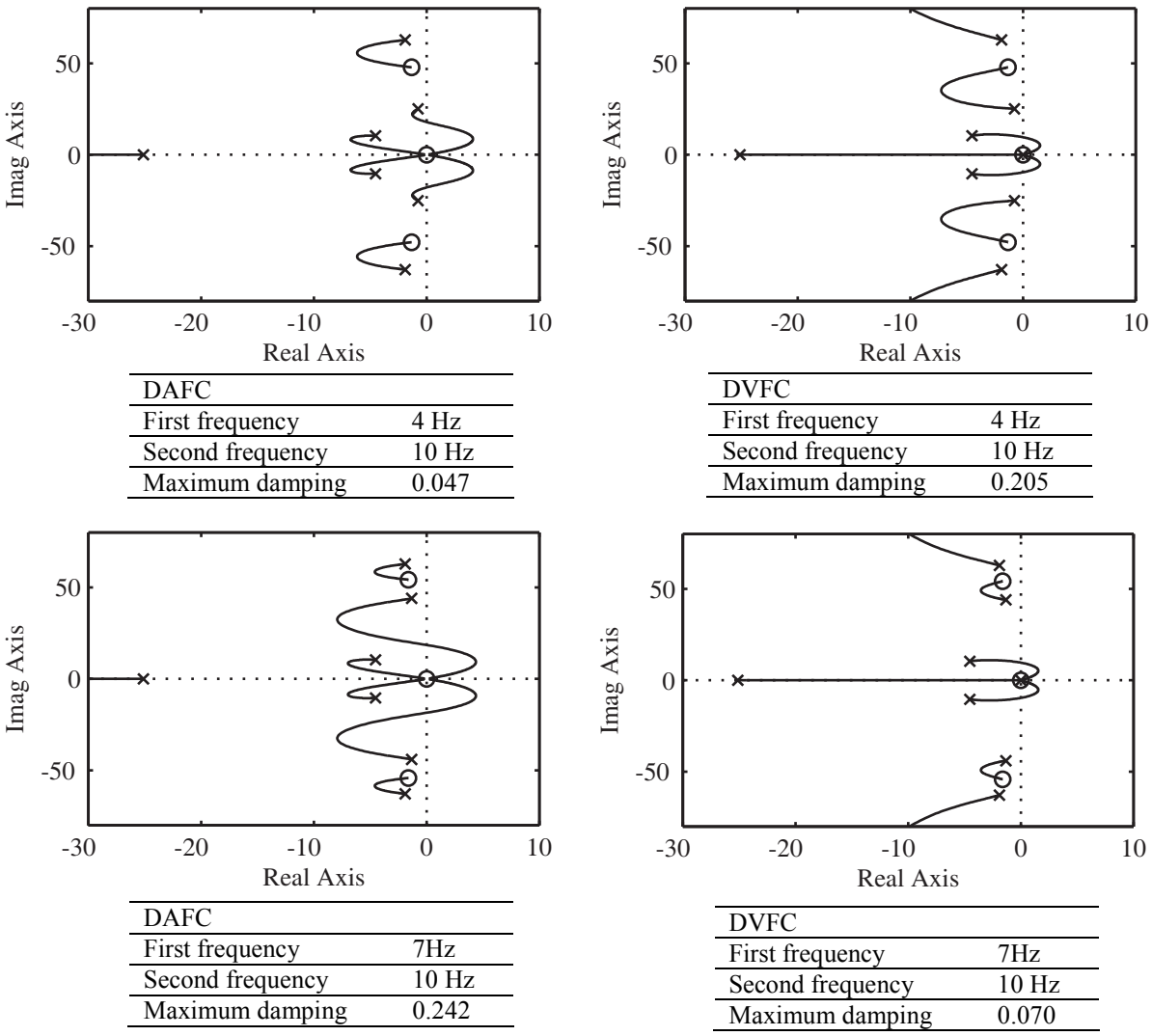

DAFC	
First frequency	4 Hz
Second frequency	10 Hz
Maximum damping	0.047

DVFC	
First frequency	4 Hz
Second frequency	10 Hz
Maximum damping	0.205

DAFC	
First frequency	7Hz
Second frequency	10 Hz
Maximum damping	0.242

DVFC	
First frequency	7Hz
Second frequency	10 Hz
Maximum damping	0.070

Fig. 3. Examples of root loci. (×) pole; (o) zeros.

The possible values of γ that provide the aforementioned features can be bound through the departure angle at zero gain of the locus corresponding to the fundamental floor vibration mode. This angle must point to negative values of the real axis. To obtain this angle, the argument equation of the closed-loop characteristic equation is used. That is, any point s_1 of a specific trajectory verifies the following equation [16]

$$\sum_{i=1}^{n_z} \angle\left(s_1 + z_i\right) - \sum_{j=1}^{n_p} \angle\left(s_1 + p_j\right) = \pm\left(2k+1\right)\pi \text{ with } k \in \mathbb{N}, \tag{10}$$

in which n_z is the number of zeros, n_p is the number of poles and $\angle\left(s_1 + z_i\right)$ and $\angle\left(s_1 + p_j\right)$ are the angles of vectors drawn from the zeros and poles, respectively, to point s_1. The departure angle can be determined by letting s_1 be a point very close to one of the poles of the fundamental floor vibration

mode. As an example, the dominant dynamics are considered without the direct compensator. Note that the inclusion of the direct compensator and high floor vibration modes adds pairs of zeros and poles that are very close together such that their effect in the root locus can be neglected. Fig. 4 shows the map of zeros and poles under the aforementioned conditions. Eq. (10) can be written as follows

$$\left(\beta_1+\beta_2+\beta_3+\beta_4\right)-\left(\alpha_1+\alpha_2+\alpha_3+\alpha_4+\alpha_5\right)=\pm\left(2k+1\right)\pi \text{ with } k\in\mathbb{N}. \tag{11}$$

If it is considered that the damping of the fundamental vibration mode is $\xi_1\simeq 0$, the following assumptions can be done: $\beta_1=\beta_2=\beta_3\simeq\pi/2$ and $\alpha_5\simeq\pi/2$. Therefore, Eq. (11) can be rewritten as

$$\beta_4-\left(\alpha_1+\alpha_2+\alpha_3+\alpha_4\right)=\pm 2k\pi \text{ with } k\in\mathbb{N}. \tag{12}$$

Considering transfer functions (2) and (3), the angles α_1, α_2 and α_3 are of the following form

$$\alpha_1=\operatorname{atan}\left(\frac{\omega_1}{\varsigma_A\omega_A}-\frac{\sqrt{1-\varsigma_A^2}}{\varsigma_A}\right),\ \alpha_2=\operatorname{atan}\left(\frac{\omega_1}{\varsigma_A\omega_A}+\frac{\sqrt{1-\varsigma_A^2}}{\varsigma_A}\right),\ \text{and } \alpha_3=\operatorname{atan}\left(\frac{\omega_1}{\varepsilon}\right). \tag{13}$$

Considering transfer function (2) and (9), the angle β_4 is obtained as

$$\beta_4=\operatorname{atan}\left(\frac{\omega_1}{\gamma}\right). \tag{14}$$

Then, by imposing a minimum $\alpha_{4,\min}$ and a maximum $\alpha_{4,\max}$ value of the departure angle α_4 of the fundamental floor vibration mode, a couple of values of β_4 can be obtained

$$\beta_{4,\min}=-2\pi+\left(\alpha_1+\alpha_2+\alpha_3+\alpha_{4,\min}\right),\ \beta_{4,\max}=-2\pi+\left(\alpha_1+\alpha_2+\alpha_3+\alpha_{4,\max}\right), \tag{15}$$

in which it is assumed $k=1$. Therefore, the variation interval of β_4 is derived as follows

$$\beta_4\in\left(\max\left(0;\beta_{4,\min}\right),\min\left(\pi/2;\beta_{4,\max}\right)\right), \tag{16}$$

and using Eq. (14), the corresponding variation interval of $\gamma\in\left(\gamma_{\min},\gamma_{\max}\right)$ is determined. The final value of γ must be chosen so that the attractor properties of the zero are focussed on the fundamental floor vibration mode.

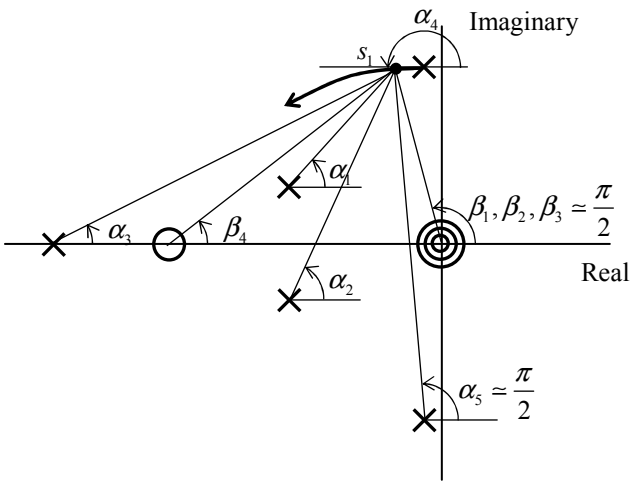

Fig. 4. Departure angle of the locus corresponding to the fundamental floor vibration mode (not to scale). (×) pole; (o) zeros.

3.3. Stability

Stability is the primary concern in any active control system applied to civil engineering structures, mainly due to safety and serviceability reasons. The control scheme of Fig. 1, assuming that the nonlinear element $f(\ddot{y}_c)$ is a saturation nonlinearity, is analysed in this section. The nonlinear element can be written as

$$f(\ddot{y}_c(t)) = \begin{cases} K_c \ddot{y}_c(t) & |\ddot{y}_c(t)| \le V_s/K_c \\ V_s sign(\ddot{y}_c(t)) & |\ddot{y}_c(t)| > V_s/K_c \end{cases}, \tag{17}$$

where K_c is the control gain and V_s is the maximum allowable control voltage to the actuator (saturation level). The saturation nonlinearity is introduced to avoid actuator saturation and to keep the system safe under any excitation and independent of selection of control parameters. The stability can be studied using the Describing Function (DF) tool in its basic form [18]. Firstly, the total transfer function of the linear part (Eqs. (2), (3), (6) and (9)) is obtained (see Fig .1)

$$G_T(j\omega) = C_D(j\omega) G_A(j\omega) \tilde{G}(j\omega) C_F(j\omega). \tag{18}$$

Then, from the root locus of $G_T(j\omega)$, the limit gain $K_{c,\text{limit}}$ for which the closed-loop system becomes unstable is derived. This is the minimum value of the control gain for which at least one of the loci intersects the imaginary axis.

Secondly, the DF, denoted by $N(A,\omega)$, for the nonlinear element is obtained. The DF is the ratio between the fundamental component of the Fourier series of the nonlinear element output and a sinusoidal

input given by $x(t) = A\sin(\omega t)$. If the nonlinearity is hard, odd and single-valued (the case of saturation nonlinearity), the DF depends only on the input amplitude $N(A,\omega) = N(A)$, i.e., it is a real function. The DF for a saturation nonlinearity is [18]

$$N(A) = \begin{cases} K_c & A \le a \\ \dfrac{2K_c}{\pi}\left[\arcsin\left(\dfrac{a}{A}\right) - \dfrac{a}{A}\sqrt{1-\dfrac{a^2}{A^2}}\right] & A > a \end{cases}, \tag{19}$$

with $a = V_s/K_c$ (see Eq. (17)). The normalized DF $N(A)/K_c$ (19) is plotted in Fig. 5a as a function of A/a. If the input amplitude is in the linear range ($A \le a$), $N(A)$ is constant and equal to the control gain $N(A) = K_c$. $N(A)$ then decreases as the input amplitude increases when $A > a$. That is, saturation does not occur for small signals and it reduces the ratio of the output to input as the input increases.

Thirdly, the extended Nyquist criterion using the DF is applied

$$G_T(j\omega) = -1/N(A). \tag{20}$$

Each solution of Eq. (20) predicts a limit cycle behaviour. The total transfer function $G_T(j\omega)$ will intersect the real axis at $-1/K_{c,\text{limit}}$. With regards to the plot of $-1/N(A)$, it will start at $-1/K_c$ and go to $-\infty$ as A increases. Depending on the value of K_c, both plots $G_T(j\omega)$ and $-1/N(A)$ can intersect. Fig. 5b illustrates this fact for an example extracted from [12]. The conclusion is that: if $K_c < K_{c,\text{limit}}$, the system is asymptotically stable and goes to zero vibration (no intersection); otherwise, a limit cycle is predicted (intersection). Such a limit cycle is deduced to be stable by using the limit cycle stability criterion [18]. The properties of the limit cycle, frequency and amplitude, can be obtained by Eq. (20) particularised to the intersection point. It is not the objective of this work to study the limit cycle behaviour; although, it is important to establish its conditions to appear in order to avoid it.

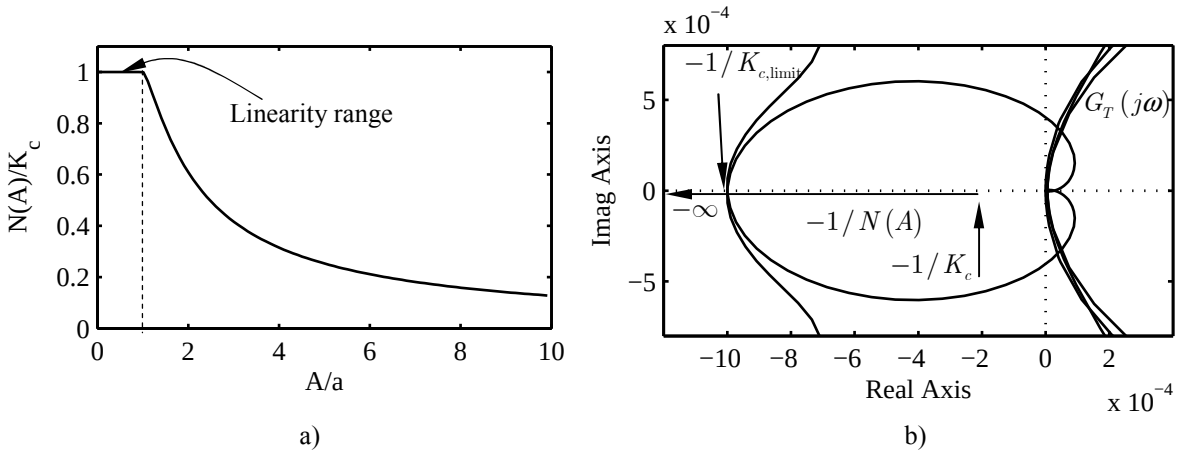

Fig. 5. a) DF for the saturation nonlinearity. b) Nyquist diagram of $G_T(j\omega)$ and $-1/N(A)$.

3.4. Design process

The design process of the control scheme represented in Fig. 1 can be summarised in the following steps:

Step 1: Identify the actuator G_A and floor dynamics $\tilde{G}$.

Step 2: Design the direct compensator (phase-lead) C_D accounting for the actuator stroke saturation. It is proposed that this design is carried out following the procedure described in Section 3.1.

Step 3: Design the feedback (phase-lag) compensator C_F to increase the damping and robustness with respect to stability and performance of the closed-loop system by following Section 3.2.

Step 4: Design the nonlinear element $f(\ddot{y}_c)$ according to stability and performance. If $f(\ddot{y}_c)$ is a saturation nonlinearity, take a saturation value to avoid actuator force overloading and select a suitable gain K_c using the root locus method.

4. Implementation of the AVC system on an office floor

This Section presents the design and practical implementation of an AVC system based on the procedure presented in Section 3 on an in-service open-plan office floor sited in the North of England.

4.1. Floor description and modal properties

The test structure is a composite steel-concrete floor in a steel frame office building. A plan of the floor is shown in Fig. 6a, in which the measurement points used for the experimental modal analysis (EMA) are indicated. Columns are located along the two sides of the building (without point numbers) and along the centreline (18-27-end), at every other test point (TP) location (i.e, 18, 20, 22, etc.). Fig 6b shows a photograph from TP 44 towards TP 28 and Fig. 6c shows a photograph from TP 12 towards TP 01. The EMA of this structure is explained in detail in [19] so only the key results are presented here. The floor is considered by its occupants to be quite lively, but not sufficiently lively to attract complaints. Special attention was paid to TP 04 and its surroundings because it was perceived to be a particularly lively location on the floor. Because the vibration perception was particularly acute at this point, this was the initial candidate for the installation of the AVC system.

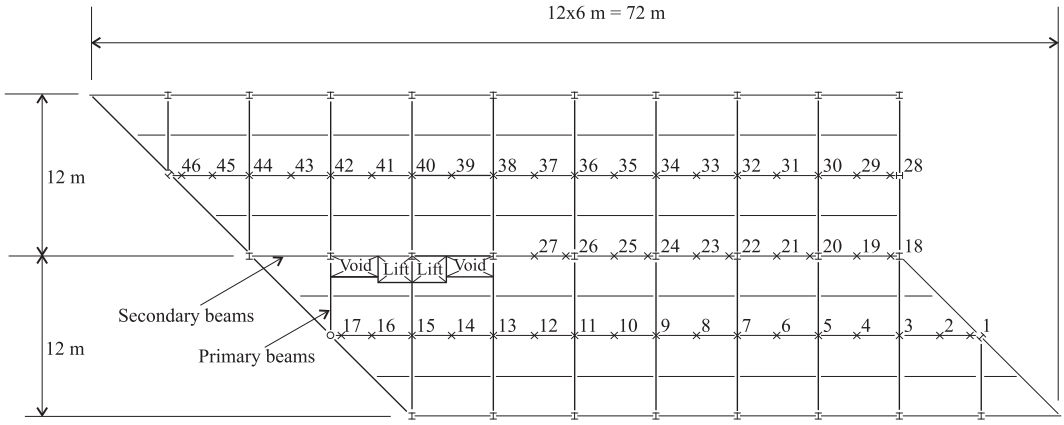

a)

b) c)

Fig. 6. Test structure. a) Plan of the floor (not to scale); (×) measurement point used in the EMA. b) View from TP 44 towards TP 28. c) View from TP 12 to TP 01.

A multi-input multi-output modal testing was carried out with four excitation points placed at TPs 04, 07, 31 and 36 and responses measured at all TPs. The artificial excitation was supplied by APS Dynamics Model 400 electrodynamic shakers (Fig. 7b) and responses were measured by QA750 force-balance accelerometers (Fig. 7c). Fig 7a shows a photograph of the multishaker modal testing carried out. Fig. 8 shows the magnitudes of the point accelerance FRFs acquired. Interestingly, the highest peak occurs at TP 04 at approximately 6.4 Hz, which was the point on the structure where the response was subjectively assessed to be highest. Parameter estimation was carried out using the multiple reference orthogonal polynomial algorithm already implemented in ME'scope suite of software. Fig. 9 shows the estimated vibration modes which are dominant at TP 04.

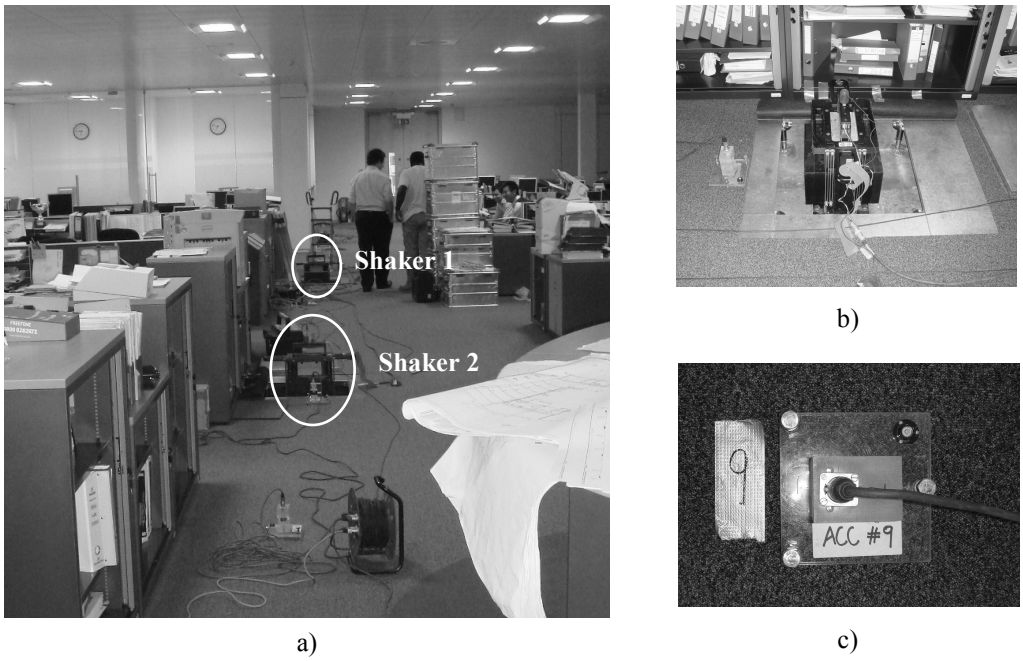

a) b) c)

Fig. 7. a) Multishaker modal testing of the floor structure. b) APS Dynamics Model 400 electrodynamic shaker. c) QA750 force-balance accelerometer.

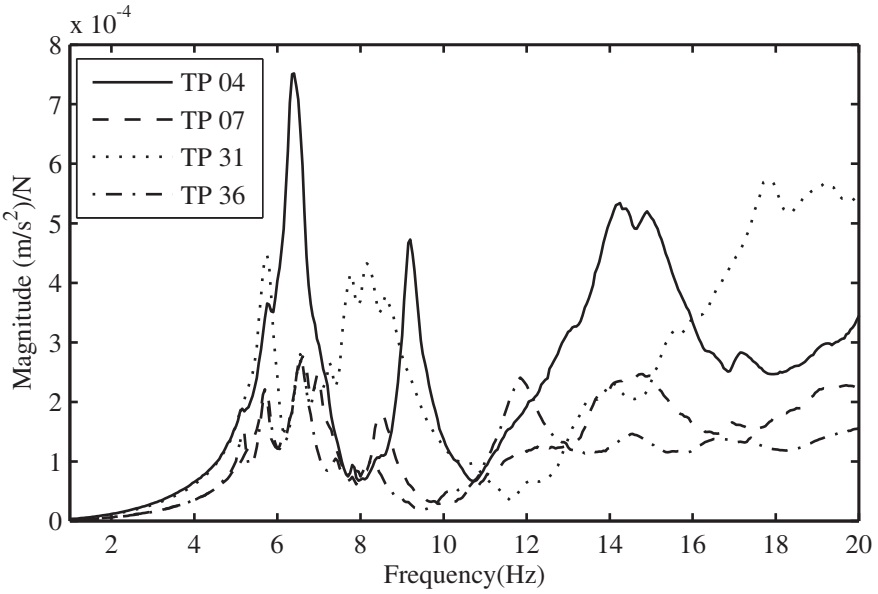

Fig. 8. Magnitudes of the point accelerance FRFs at TP 04, 07, 31 and 36.

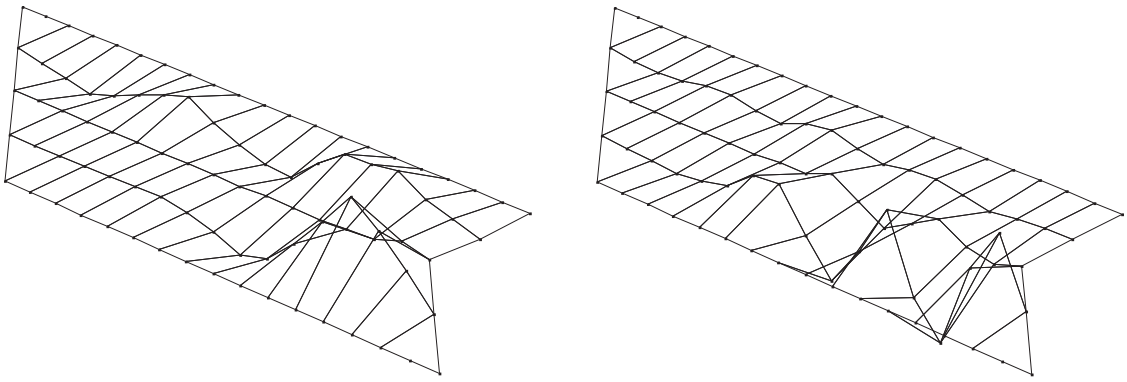

a) b)

Fig. 9. Estimated vibration modes prone to be excited by human walking at TP 04. a) Vibration mode at 6.37 Hz. b) Vibration mode at 9.19 Hz.

4.2. System dynamics and experimental setup

The AVC system was placed at TP 04. The floor dynamics at the AVC location (Eq. (2)) and the actuator dynamics (Eq. (3)) were identified. Using the modal parameters obtained from the EMA, the transfer function of the floor was modelled considering three vibration modes $N = 3$ in the frequency range of 0–20 Hz

$$\tilde{G}(s) = \frac{4.49 \cdot 10^{-5} s^2}{s^2 + 2.36s + 1627} + \frac{1.74 \cdot 10^{-5} s^2}{s^2 + 2.09s + 3341} + \frac{1 \cdot 10^{-4} s^2}{s^2 + 17.59s + 7738}. \quad (21)$$

Fig. 10 shows the magnitude and phase response of the modelled (Eq. (21)) and experimental frequency response function (FRF). The model was found to capture the floor dynamics with sufficient accuracy in the frequency bandwidth of interest.

The proof-mass actuator was an APS Dynamics Model 400 electrodynamic shaker (operated in inertial mode) with an inertial mass of 30.4 kg. The actuator model was obtained to be

$$G_A(s) = \frac{12600s^2}{s^3 + 62.16s^2 + 728.6s + 6573}. \quad (22)$$

The natural frequency of the actuator was estimated as 1.80 Hz and the pole that provides the low pass property was estimated to be $\varepsilon = 50.26$ (Eq. (3)). A picture of the actuator, which was installed on the main floor, is shown in Fig. 11.

The floor response was measured by a piezoelectric accelerometer (Endevco 7754A-1000) mounted on a levelled baseplate and installed on the main floor (see Fig. 11). The dynamics introduced by the sensor were not considered in the control scheme since they are negligible for the bandwidth of interest. The controller hardware completes the experimental setup. It comprises of a digital computer with a low cost National Instruments PCI-6030E DAQ card installed, which was used to compute digitally the control law.

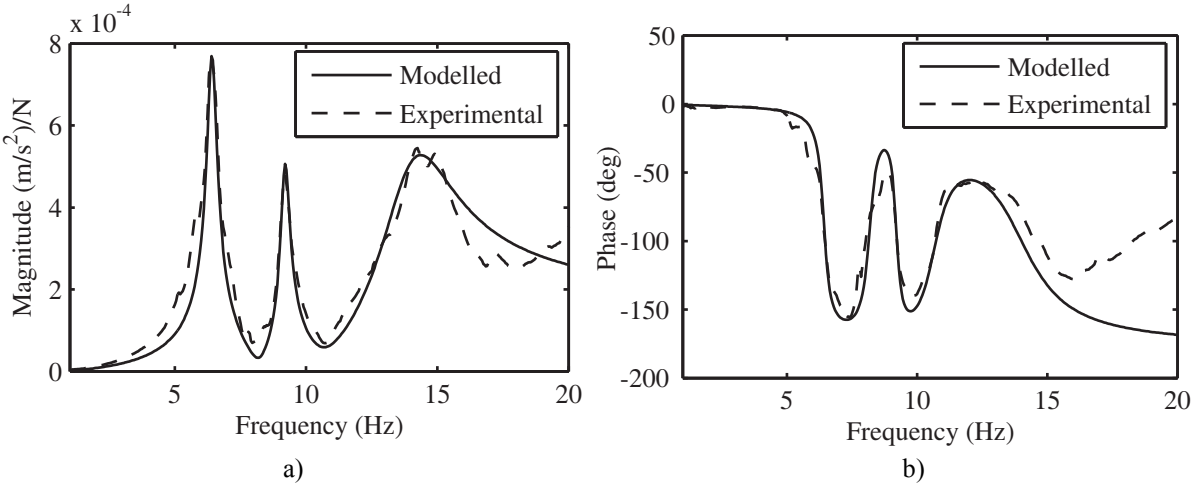

Fig. 10. Transfer function at TP04 $\tilde{G}(s)$. a) Magnitude. b) Phase.

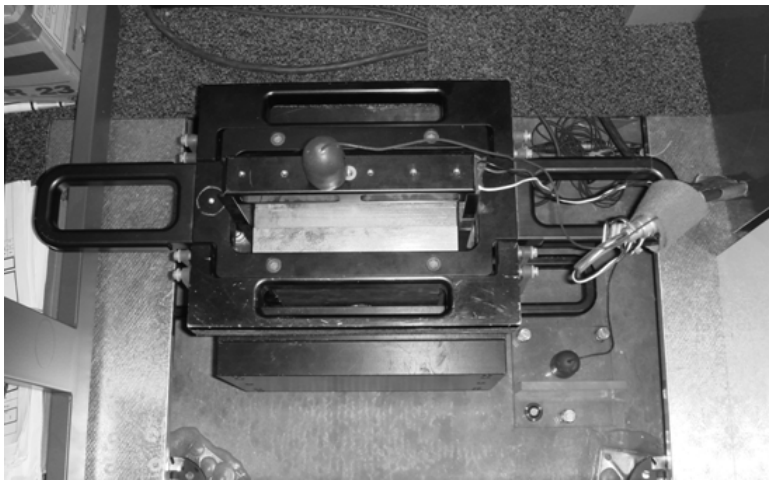

Fig. 11. Actuator and sensor (mounted on a levelled baseplate) installed on the main floor (top view).

4.3. Selection of control parameters

The purpose of this section is to obtain the parameters of compensators C_D and C_F in the continuous time domain following Section 3. As mentioned previously, during real-time control, a digital computer was used for the on-line calculation of the control signal $V(t)$. The system output was sampled with a period $\Delta t = 0.001$ s and the control signal was calculated once every sampling period. Then, the discrete-time control signal was converted into a zero-order-hold continuous-time signal. Likewise, the continuous transfer functions of the compensators were converted to discrete transfer function using the zero-order-hold approximation.

Firstly, C_D was obtained. From (22), the transfer function G_d (Eq. (4)) was derived. By assuming a value of $d = 0.05$ m, which is appropriate considering the actual stroke limit of the actuator is 0.075 m, its magnitude $\left|\hat{G}_d(j\omega)\right|$ (Eq. (5)) was obtained with $\hat{\omega} = 14.74$ rad/s. The compensator parameters were thus derived from the optimisation problem (8) in which it was assumed $\omega_L = 1.25$ rad/s, $\omega_U = 62.83$ rad/s and $\lambda_{\max} = \eta_{\max} = \varepsilon = 50.26$. The control parameters were then found to be $\lambda = 6.87$ and $\eta = 14.34$.

Secondly, the feedback compensator C_F (Eq. (9)) was obtained. Taking into account the dominant dynamics: G_A, C_D and the fundamental floor vibration mode of (21), and restricting the departure angle of the locus corresponding to the fundamental floor vibration mode $\alpha_4 \in (180, 225)$ deg (see Fig. 4), then the angle corresponding to the zero of the compensator β_4 can be bounded. It was obtained

$\beta_4 \in (10.24, 55.24)$ deg and consequently $\gamma \in (27.9, 223.2)$ using Eq. (14). A value of $\gamma = 55$ was chosen since it must be higher than the inferior limit but it should not be so high that the attractor effect of the zero is focussed on the fundamental vibration mode. The root locus technique was used here. The root locus of G_T (Eq. (18)) for CAFC is plotted in Fig. 12. It can be observed that the linear system might be critically damped for the fundamental floor vibration mode. For comparison purposes, Fig. 13 shows the corresponding root locus for DAFC and DVFC. It can be observed that DAFC provides very poor damping augmentation and the floor dynamics become unstable even for very small control gains. On the other hand, DVFC provides much better properties than DAFC; however, CAFC improves substantially the desirable properties for the linear system.

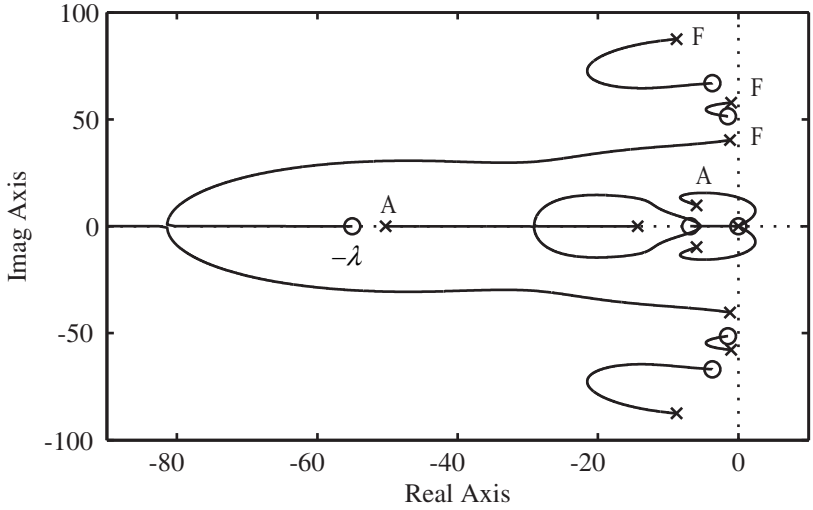

Fig. 12. Root locus of the total transfer function G_T for CAFC. (×) pole; (o) zero; (F) floor; (A) actuator.

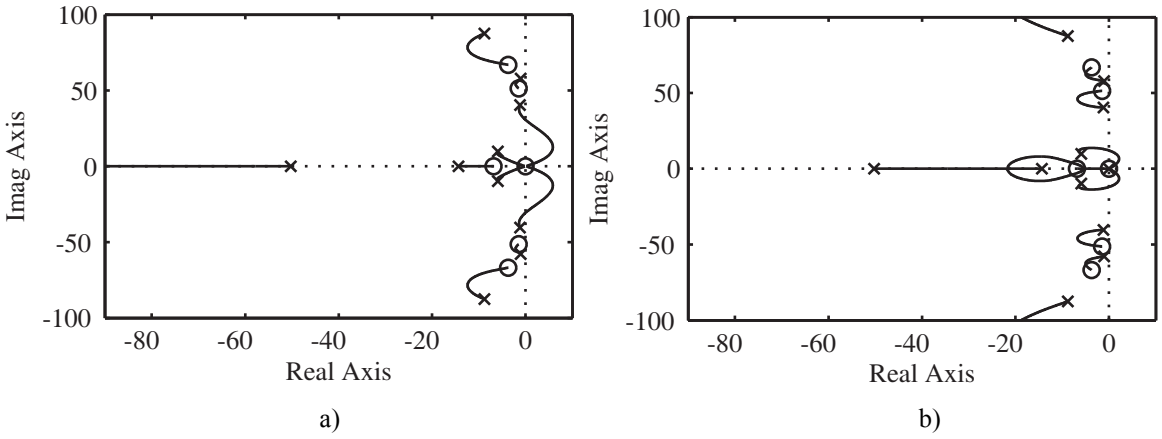

Fig. 13. a) Root locus of the total transfer function G_T for DAFC. b) Root locus of G_T for DVFC. (×) pole; (o) zero.

Finally, the nonlinear element is chosen as a saturation nonlinearity (17) with $V_s = 0.5$ V, which is a convenient value to avoid actuator force overloading at any frequency of the excitation. Therefore, the stability is guaranteed just by taking a safe control gain $K_c < K_{c,\text{limit}}$. The limit gain was predicted to be $K_{c,\text{limit}} = 44.4 \ \text{V}/\left(\text{m}/\text{s}^2\right)$. Values of damping of the actuator poles smaller than 0.30 are not recommended [17]. This damping is reached for $K_c = 18.6 \ \text{V}/\left(\text{m}/\text{s}^2\right)$. Therefore, K_c must not be higher than $18.6 \ \text{V}/\left(\text{m}/\text{s}^2\right)$.

4.4. Walking tests

The AVC system was assessed firstly by carrying out several simulations using different values of the control gain K_c. MATLAB/Simulink was used for this purpose. The control scheme shown in Fig. 1 was simulated using the transfer function models given by Eqs. (6) and (10) with the parameters obtained in Section 4.3 and Eqs. (21) and (22) obtained from FRF identifications. The control scheme was perturbed by a real walking excitation obtained from an instrumented treadmill [20] ($p(t)$ in Fig. 1). Table 1 shows the results obtained. Two different pacing frequencies (1.58 and 2.12 Hz) were used in such a way that the first floor vibration mode might be excited by the third or the fourth harmonic. The results are compared in terms of the maximum transient vibration value (MTVV) calculated from the 1 s running RMS acceleration and from the vibration dose value (VDV) obtained from the total period of the excitation [21]. The BS 6841 W_b weighted acceleration was used for both measures [22]. The results predicted that the AVC was quite insensitive to the gain value and that the reduction in vibration was approximately 60 % for slow walking (1.58 Hz) and 53 % for fast walking (2.12 Hz) in terms of MTVV. The results in terms of the VDV provide similar reductions as for the MTVV.

Actual walking tests were carried out on the test structure using the same walking excitation frequencies as in the simulations. The walking path consisted of walking from TP 01 to TP 09 and then back from TP 09 to TP 01 (see Fig. 6). A gain of $K_c = 15 \ \text{V}/\left(\text{m}/\text{s}^2\right)$ was found to give good performance so that was used in the experiments. Fig. 14 shows BS 6841 W_b weighted response time histories (including the 1s RMS and the cumulative VDV), uncontrolled and controlled, for a pacing frequency of 1.58 Hz, which was controlled using a metronome set to 95 beats per minute (bpm). The MTVV was reduced from $0.031 \ \text{m}/\text{s}^2$ to $0.010 \ \text{m}/\text{s}^2$, a reduction of 68 %, and the VDV was reduced

from $0.050\ \mathrm{m/s^{1.75}}$ to $0.019\ \mathrm{m/s^{1.75}}$, a reduction of 62 %. Fig. 15 shows the response time histories for a pacing frequency of 2.12 Hz (127 bpm). The achieved reduction in terms of the MTVV was 52 %, from $0.033\ \mathrm{m/s^{2}}$ to $0.016\ \mathrm{m/s^{2}}$, and in terms of the VDV was 51 %, from $0.057\ \mathrm{m/s^{1.75}}$ to $0.028\ \mathrm{m/s^{1.75}}$. It was observed that the experimental reductions agreed very well with the numerical predictions (see Table 1).

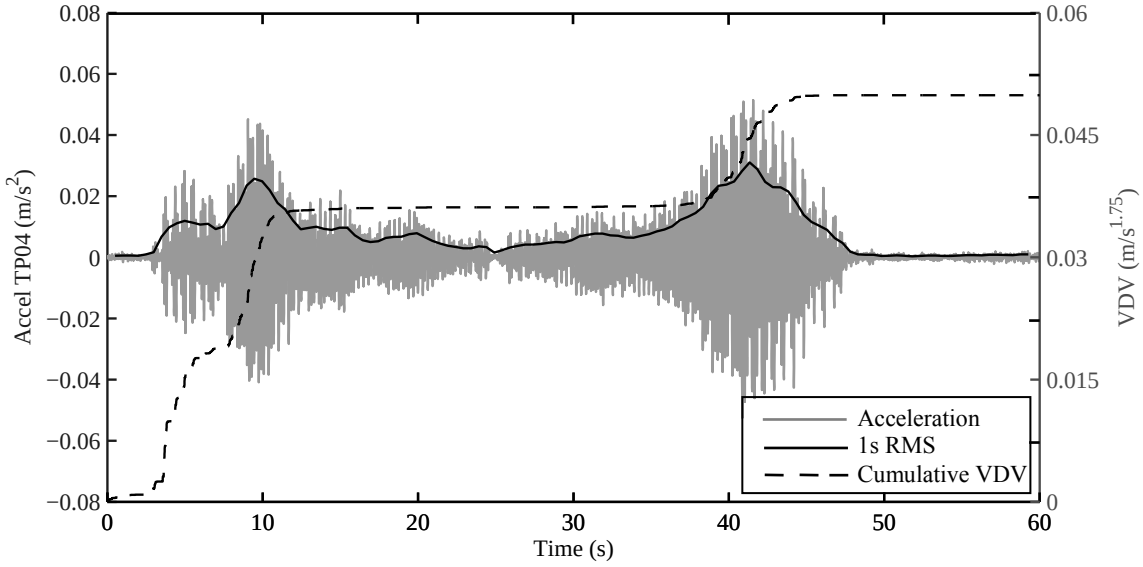

a)

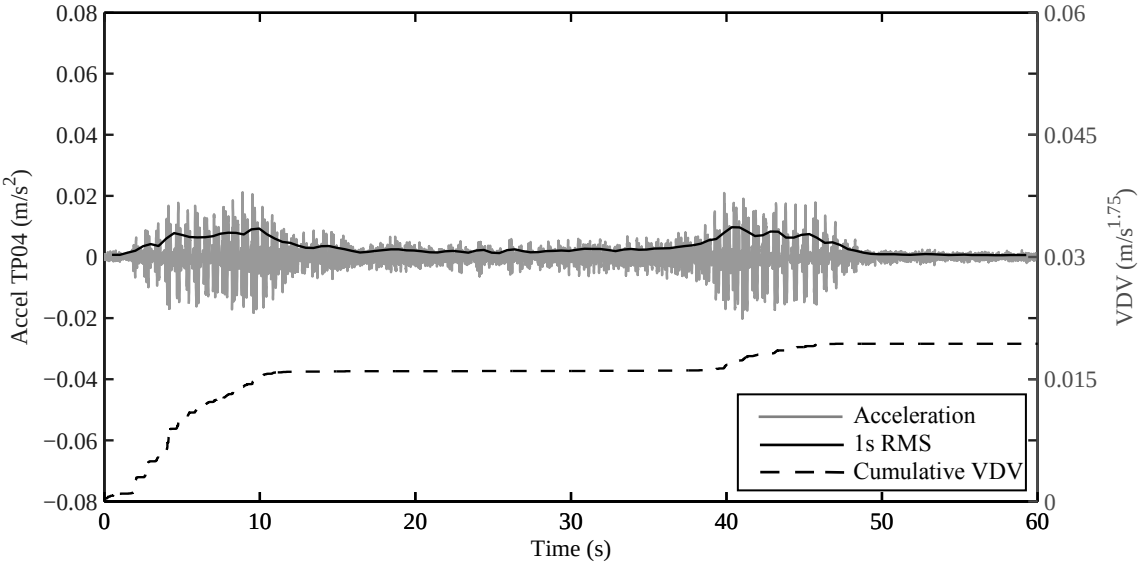

b)

Fig. 14. Experimental results. Walking at 1.58 Hz (95 bpm). a) Uncontrolled $\mathrm{MTVV} = 0.031\ \mathrm{m/s^{2}}$ and $\mathrm{VDV} = 0.050\ \mathrm{m/s^{1.75}}$. b) Controlled $\mathrm{MTVV} = 0.010\ \mathrm{m/s^{2}}$ and $\mathrm{VDV} = 0.019\ \mathrm{m/s^{1.75}}$.

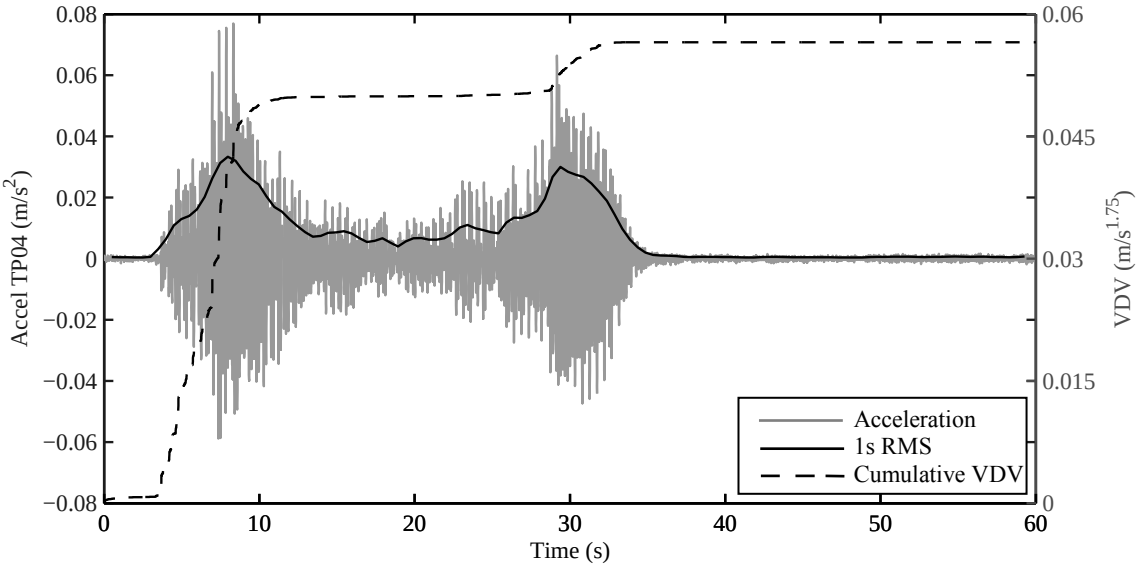

a)

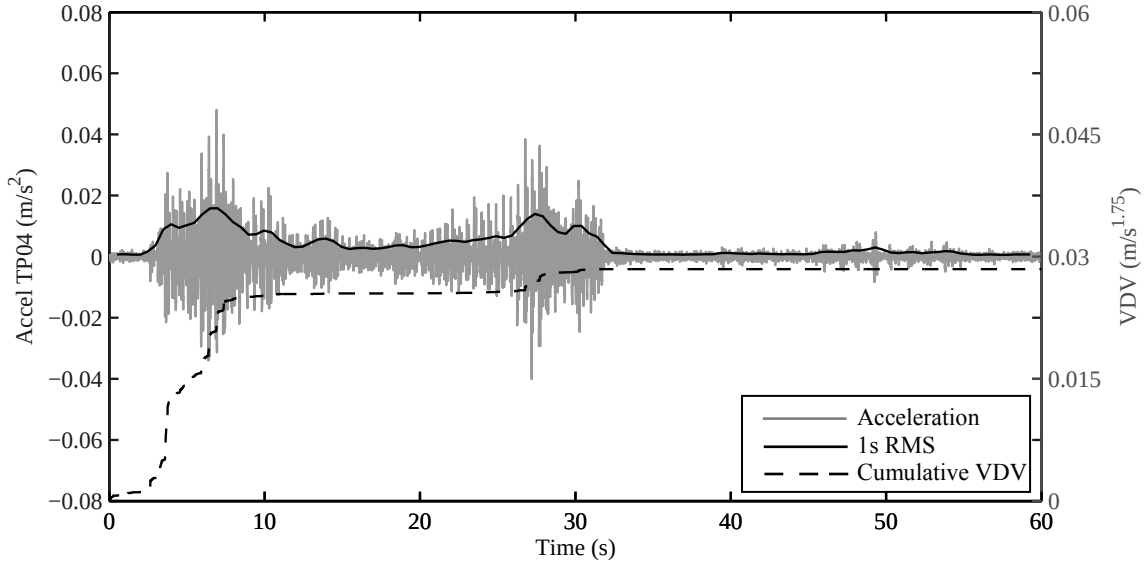

b)

Fig. 15. Experimental results. Walking at 2.12 Hz (127 bpm). a) Uncontrolled $\mathrm{MTVV} = 0.033\ \mathrm{m/s^2}$ and $\mathrm{VDV} = 0.057\ \mathrm{m/s^{1.75}}$. b) Controlled $\mathrm{MTVV} = 0.016\ \mathrm{m/s^2}$ and $\mathrm{VDV} = 0.028\ \mathrm{m/s^{1.75}}$.

4.5. In-service monitoring

Continuous whole-day monitoring was carried out to assess the vibration reduction achieved by the AVC system. The acceleration was measured from 6:00 am to 6:00 pm during four working days, two without and two with the AVC system. The R-factor was used to quantify the vibration reduction. This factor is defined as the ratio between the 1 s running RMS of the BS 6841 W_b weighted acceleration

response and 0.005 m/s^2 [23]. Fig. 16 shows the percentage of time during which the R-factor is over 1, 2, 3, 4 and 5. The values shown in the figure are the mean values between the two corresponding days. It was observed that the time for which the R-factor was over 1 was reduced by 60 % and the time for which it was over 4 was significantly reduced by over 97 %. Note that the second reduction is very important since an R-factor of 4 is a commonly used vibration limit for a high quality office floor [24]. Hence, these results clearly illustrate the effectiveness of the AVC system designed. In addition, the cumulative VDV was also calculated for the same exposure to vibration and using the W_b weighted acceleration. The VDV obtained when the AVC system was disconnected was $0.162\ m/s^{1.75}$ whereas such a value was $0.101\ m/s^{1.75}$ when the system was engaged. The reduction achieved was almost 40 %. Note that the VDV is much more strongly influenced by vibration magnitude than duration [21]. This fact results in less vibration reduction in terms of the VDV than using the MTVV.

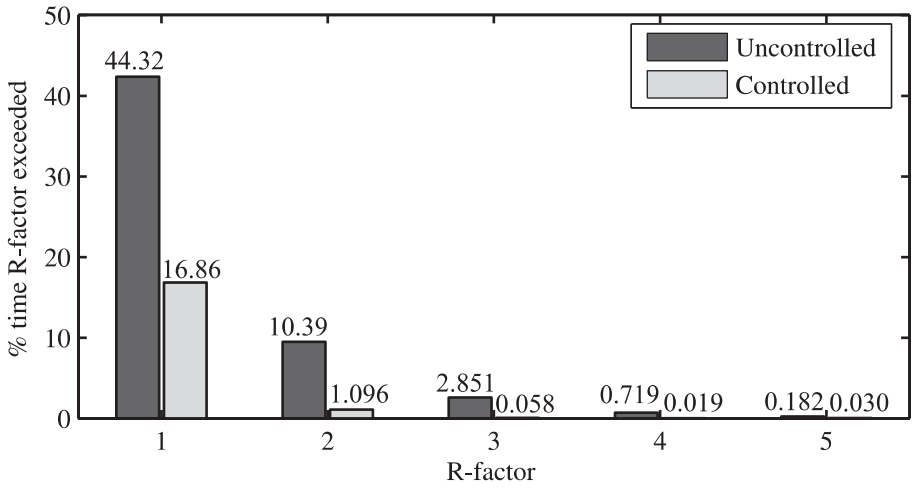

Fig. 16. Whole-day monitoring: percentage of time of exceedance of R-factors.

5. Conclusions

The active cancellation of floor vibrations induced by human motions has been considered throughout this paper. Previous researchers have used velocity feedback. However, it has been shown that the use of velocity feedback might not be a good option since the actuator dynamics influence importantly the floor dynamics in such a way that the interlacing property of poles and zeros is no longer fulfilled. Instead of using velocity feedback, this work proposes to feedback the acceleration (which is the actual measured output) and applies a first-order compensator (phase-lag network) conveniently designed in order to achieve significant relative stability and damping. Note that the compensator could be equivalent

to an integrator circuit leading to velocity feedback, depending on the interaction between actuator and floor dynamics. Moreover, the proposed control scheme is completed by a phase-lead network to avoid actuator resonance behaviour and a nonlinear element to account for actuator overloading. A simple step-by-step procedure has been proposed for the design of the controller parameters.

An AVC system designed based on the proposed control scheme has been tested in an in-service open-plan floor. This floor had a vibration mode at 6.4 Hz which was the most likely to be excited. This mode had a damping ratio of 3% and a modal mass of approximately 20 tonnes. Reductions of approximately 60 % were observed in MTVV and cumulative VDV for controlled walking tests. For in-service whole-day monitoring, the amount of time that an R-factor of 4 was exceeded, which is a commonly used vibration limit for high quality office floor, was reduced by over 97 %. Additionally, the cumulative VDV was interestingly reduced over 40 %.

Future works should address the development of more compact and economically interesting actuators to be used for the active control of floor vibrations. Then, active control may be a viable and economic solution for non-acceptable floor vibrations.

Acknowledgments

The authors would like to acknowledge the financial support of Conserjería de Educación y Ciencia of Junta de Comunidades de Castilla-La Mancha and European Social Fund. The authors are very grateful to Jeremy Wells of WSP Buildings for his support for this work. The assistant of the research student Donald Nyawako from the Department of Civil and Structural Engineering, The University of Sheffield, is also gratefully acknowledged.

References

[1] Bachman H. Case studies of structures with man-induced vibrations. Journal of Engineering Structures 1992; 118(3): 631–47.

[2] Setareh M, Hanson RD. Tuned mass damper to control floor vibration from humans. Journal of Structural Engineering 1992; 118(3): 741–62.

[3] Setareh M. Floor vibration control using semi-active tuned mass dampers. Canadian Journal of Civil Engineering 2002; 29(1): 76–84.

[4] Hanagan LM, Murray TM, Premaratne K. Controlling floor vibration with active and passive devices. The Shock and Vibration Digest 2003; 35(5): 347–65.

[5] Nyawako D, Reynolds P. Technologies for mitigation of human-induced vibration in civil engineering structures. The Shock and Vibration Digest 2007; 36(6): 465–93.

[6] Ebrahimpour A, Sack RL. A review of vibration serviceability criteria for floor structures. Computers and Structures 2005; 83: 2488–94.

[7] Hanagan LM, Murray TM. Active control for reducing floor vibrations. Journal of Structural Engineering 1997; 123(11): 1497–1505.

[8] Hanagan LM, Murray TM. Experimental implementation of active control to reduce annoying floor vibration. Engineering Journal 1998; 35(4): 123–27.

[9] Balas MJ. Direct velocity feedback control of large space structures. Journal of Guidance and Control 1979; 2(3): 252–53.

[10] Preumont A. Vibration control of active Structures: An introduction, Kluwer Academic, Dordrecht, The Netherlands, 1997.

[11] Moutinho C, Cunha A, Caetano E. Implementation of an active damping system to reduce harmonic vibrations in a 3DOF physical model. In: Proceedings of II ECCOMAS Thematic Conference on Smart Structures and Materials 2005; Lisbon, Portugal.

[12] Diaz IM, Nyawako DS, Reynolds P. On-off nonlinear velocity feedback control for cancelling floor vibrations. In: Proceedings of the 4th European Conference on Structural Control 2008; St. Petersburg, Russia, 1: 175–82.

[13] Chung LY, Jin TG. Acceleration feedback control of seismic structures. Engineering Structures 1998; 20(1); 62–74.

[14] Nyawako DS, Reynolds P. Active control of human induced floor vibrations. In: Proceedings of the 26th International Modal Analysis Conference 2008; Orlando, Florida, USA.

[15] APS. Instruction Manual Electro-Seis Model 400 Shaker, APS Dynamics, USA.

[16] Bolton W. Control engineering, Logman, United Kingdom, 1998.

[17] Hanagan LM. Active floor vibration system, United States Patent 6874748, 2005.

[18] Slotine JJ, Li W. Applied non linear control, Prentice-Hall, 1991, Chapter 5.

[19] Reynolds P, Diaz IM, Nyawako DS. Vibration testing and active control of an office floor. In: Proceedings of the 27th International Modal Analysis Conference 2009; Orlando, Florida, USA.

[20] Brownjohn JMW, Pavic A, Omenzetter P. A spectral density approach for modelling continuous vertical forces on pedestrian structures due to walking. Canadian Journal of Civil Engineering 2004; 31(1); 65–77.

[21] BS. BS 6472, Guide to evaluation of human exposure to vibration in buildings. Part 1: Vibration sources other than blasting, British Standards Institution, United Kingdom, 2008.

[22] BS. BS 6841 Measurement and evaluation of human exposure to whole-body mechanical vibration and repeated shock, British Standards Institution, United Kingdom, 1987.

[23] Wyatt TA. Design guide on the vibration of floors, The Steel Construction Institute, United Kingdom, 1989.

[24] Pavic A, Willford M. Appendix G in Post-tensioned concrete floors design handbook–Technical Report 43, Concrete Society, Slough, United Kingdom, 2005.

Table 1

Simulation performance assessment for several control gains and walking excitation.

Control gain (V/(m/s^2))	Uncontrolled	5	10	15	20
Walking at 1.58 Hz					
MTVV[(1)] (m/s^2)	0.030	0.0122	0.0115	0.0115	0.0116
Reduction MTVV (%)	—	59	62	62	61
VDV[(2)] (m/s$^{1.75}$)	0.063	0.029	0.027	0.027	0.027
Reduction VDV (%)	—	55	58	58	57
Walking at 2.12 Hz					
MTVV[(1)] (m/s^2)	0.033	0.0154	0.0150	0.0156	0.0160
Reduction MTVV (%)	—	53	55	53	52
VDV (m/s$^{1.75}$)	0.073	0.034	0.032	0.033	0.033
Reduction VDV (%)	—	54	56	55	55

[(1)] Maximum Transient Vibration value defined as the maximum value of 1s running RMS acceleration

[(2)] Cumulative Vibration Dose Value